Inductively Coupled In-Circuit Measurement of Two-Port Admittance Parameters

Simone Negri, *Member*, Giordano Spadacini, *Senior member,* Flavia Grassi, *Senior member,* and Sergio A. Pignari, *Fellow*

***Abstract*—In-circuit impedance and admittance measurements are widely exploited in power electronics, from control stability analysis to electromagnetic interference modelling. In particular, the use of clamp-on inductive probes allows non-intrusive measurements of systems in real operating conditions. However, available methods are limited to a single port and cannot evaluate mutual impedances or admittances, hence they cannot properly characterize multiport systems described by impedance or admittance matrices. In this paper, a two-port inductively coupled in-circuit measurement method is proposed. Specifically, two inductive probes connected to a vector network analyzer define two longitudinal ports along the clamped wires of the system under test and allow measurement of its two-by-two admittance matrix. The proposed method is firstly verified with a set of known passive loads, then applied to measure the unknown admittance matrix of a single-phase motor drive system. Experimental results prove the effectiveness of the proposed method in providing accurate measurement of admittance parameters, including mutual terms, both for active and passive two-port devices. Additionally, such two-port admittance matrix measurements are suitable for the identification of the behavioral circuit model of a system, in general for any number of ports.**

***Index Terms*—In-circuit impedance measurement, In-circuit admittance measurement, behavioral models, motor drive system.**

I. Introduction

IMPEDANCE and admittance measurement methods are fundamental for the experimental characterization of components and systems frequency responses. In this respect, in-circuit measurement methods enable impedance and admittance characterizations in a wide frequency range while the system is in operation. In particular, in-circuit impedance measurements are profitably used for many applications such as power converter stability analysis, including cascaded DC/DC converters [1], high-speed railways traction systems [2], and double-fed induction generators [3], asynchronous motor turnfault [4] and interfault [5] diagnosis, battery state-of-charge estimation [6]-[8], and electromagnetic interference (EMI) modeling. The latter include design [9]-[10] and performance analysis [11]-[13] of EMI filters, and broadband behavioral modeling of converters as EMI sources [14], [15].

Three families of in-circuit impedance measurements are known, namely: voltage-current (V-I), capacitively coupled, and inductively coupled [16]. The V-I approach is based on measurements of voltage and current at the ports of the equipment under test (EUT) [17]-[19]. The capacitively coupled approach involve capacitors to attenuate dc or low-frequency functional signals while presenting a small impedance for high-frequency test signals so that impedance analyzers can perform in-circuit impedance measurements [20], [21]. Both the V-I and capacitively coupled approaches are intrusive, as they need electrical contact with the energized EUT.

Conversely, the inductively coupled approach uses inductive probes clamped on EUT cables, simplifying measurement setups and reducing potential hazards [22]-[24]. Two categories of inductively coupled methods have been developed: two-probe setup (TPS) [23]-[25] or single-probe setup (SPS) [26], [27]. The measurement instrument is usually a vector network analyzer (VNA) and additional elements may be used to enhance signal-to-noise ratio [5]. TPS was originally intended for power lines in-circuit impedance measurement [28], and was successively extended [10], [29]-[31]. SPS avoids the possible issues related to probe-to-probe coupling, as only one probe is needed, thus reducing setup complexity [13], [26]. SPS proved to be suitable for the measurement of single physical or modal impedances in a motor-drive system [13], [32], [33] and even time-varying impedances [27]. To improve the sensitivity of the SPS, one can clamp the probe on more than one turn of the EUT cable [13]. Both TPS and SPS are limited to one port, that is, a single impedance, and cannot measure mutual impedances. Consequently, no one of the available setups can be used to characterize multiport systems, which are properly described by impedance or admittance matrices.

This paper proposes an inductively-coupled, in-circuit admittance parameter measurement method, derived as a multiport extension of the SPS. This is achieved by two

Manuscript received October 9th, 2023, revised December 14th, 2023, accepted January 9th, 2024. This study was carried out within the MOST – Sustainable Mobility Center and received funding from the European Union Next-Generation EU (PIANO NAZIONALE DI RIPRESA E RESILIENZA (PNRR) - MISSIONE 4 COMPONENTE 2, INVESTIMENTO 1.4 - D.D. 1033 17/06/2022, CN00000023). This manuscript reflects only the authors' views and opinions, neither the European Union nor the European Commission can be considered responsible for them.

The Authors are with the Department of Electronics, Information and Bioengineering, Politecnico di Milano, Milan, 20133, Italy (e-mail: simone.negri@polimi.it, giordano.spadacini@polimi.it, flavia.grassi@polimi.it, sergio.pignari@polimi.it).

probes, which define two separate longitudinal ports along the clamped wires, thus allowing the determination of self and mutual admittance elements. Moreover, the choice of admittance instead of impedance brings two advantages: a) straightforward identification of the behavioral circuit model of the EUT [11], [34], and b) possible extension to any number of ports using two probes only.

The paper is structured as follows: Section II formally presents the proposed measurement setup, the underlying mathematical formulation, and the calibration procedure. In Section III, the method is implemented with specific instrumentation working in the range 150 kHz – 30 MHz, and accuracy is verified by a set of known passive loads. Section IV applies the proposed method to measurement of the in-circuit admittance matrix of a single-phase motor drive system (MDS), including the de-embedding of the power-line impedance, and the identification of a behavioral circuit model. Lastly, final conclusions and remarks are reported in Section V.

II. Proposed In-Circuit Admittance Matrix Measurement Method

A. Measurement Principle

Let us consider the setup depicted in Fig. 1, which consists of a VNA, two inductive probes, and a 2-port EUT. The target of the proposed method is to determine the 2×2 unknown admittance matrix $\mathbf{Y}_x$ of the EUT, from the knowledge of the S-parameter matrix $\mathbf{S}_m$ of the whole setup measured by the VNA, which relates the incident power waves a_1, a_2 and reflected power waves b_1, b_2, according to

$$\begin{bmatrix} b_1 \\ b_2 \end{bmatrix} = \underbrace{\begin{bmatrix} S_{m11} & S_{m12} \\ S_{m21} & S_{m22} \end{bmatrix}}_{\mathbf{S}_m} \begin{bmatrix} a_1 \\ a_2 \end{bmatrix} \tag{1}$$

To this end, $\mathbf{S}_m$ is firstly converted into the measured admittance matrix $\mathbf{Y}_m$ by

$$\mathbf{Y}_m = Z_0^{-1}\left(\mathbf{I}_2 - \mathbf{S}_m\right)\left(\mathbf{I}_2 + \mathbf{S}_m\right)^{-1} = \begin{bmatrix} \frac{1}{Z_0}\frac{1 - S_{m11} + S_{m22} - \det[\mathbf{S}_m]}{1 + S_{m11} + S_{m22} + \det[\mathbf{S}_m]} & -\frac{1}{Z_0}\frac{2S_{m12}}{1 + S_{m11} + S_{m22} + \det[\mathbf{S}_m]} \\ -\frac{1}{Z_0}\frac{2S_{m21}}{1 + S_{m11} + S_{m22} + \det[\mathbf{S}_m]} & \frac{1}{Z_0}\frac{1 + S_{m11} - S_{m22} - \det[\mathbf{S}_m]}{1 + S_{m11} + S_{m22} + \det[\mathbf{S}_m]} \end{bmatrix} \tag{2}$$

where det[.] denotes the matrix determinant, $\mathbf{I}_2$ is the 2×2 identity matrix, and Z_0 = 50 Ω is the standard S-parameter reference impedance. For the port voltages and currents defined in Fig. 1, the following relationships hold:

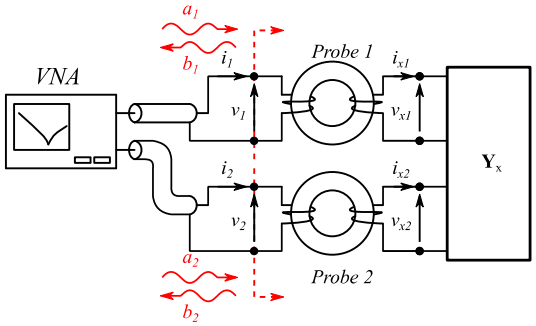

Fig. 1. Principle schematic of the considered two-port setup.

$$\begin{bmatrix} i_1 \\ i_2 \end{bmatrix} = \underbrace{\begin{bmatrix} Y_{m11} & Y_{m12} \\ Y_{m21} & Y_{m22} \end{bmatrix}}_{\mathbf{Y}_m} \begin{bmatrix} v_1 \\ v_2 \end{bmatrix} \tag{3}$$

$$\begin{bmatrix} v_1 \\ i_1 \end{bmatrix} = \underbrace{\begin{bmatrix} A_1 & B_1 \\ C_1 & D_1 \end{bmatrix}}_{\mathbf{T}_1} \begin{bmatrix} v_{x1} \\ i_{x1} \end{bmatrix} \tag{4}$$

$$\begin{bmatrix} v_2 \\ i_2 \end{bmatrix} = \underbrace{\begin{bmatrix} A_2 & B_2 \\ C_2 & D_2 \end{bmatrix}}_{\mathbf{T}_2} \begin{bmatrix} v_{x2} \\ i_{x2} \end{bmatrix}, \tag{5}$$

where $\mathbf{T}_1$, $\mathbf{T}_2$ are the transmission (also known as ABCD) matrices representing the behavioral models of probes 1 and 2, respectively, whose parameters satisfy

$$\det[\mathbf{T}_1] = \det[\mathbf{T}_2] = 1 \tag{6}$$

by virtue of reciprocity. By substituting v_1, i_1 from (4) and v_2, i_2 from (5) in (3), and accounting for property (6), after tedious yet simple algebraic calculus, the currents i_{x1}, i_{x2} can be expressed as a function of voltages v_{x1}, v_{x2}, as

$$\begin{bmatrix} i_{x1} \\ i_{x2} \end{bmatrix} = \underbrace{\begin{bmatrix} Y_{x11} & Y_{x12} \\ Y_{x21} & Y_{x22} \end{bmatrix}}_{\mathbf{Y}_x} \begin{bmatrix} v_{x1} \\ v_{x2} \end{bmatrix} \tag{7}$$

where the elements of the admittance matrix $\mathbf{Y}_x$ are finally expressed as a function of measured S-parameters and probes transmission parameters by

$$\begin{aligned} Y_{x11} &= \frac{k_1 + k_2 S_{m11} + k_2 k_7 \det[\mathbf{S}_m] + k_1 k_7 S_{m22}}{1 + k_6 S_{m11} + k_6 k_7 \det[\mathbf{S}_m] + k_7 S_{m22}} \\ Y_{x12} &= -\frac{k_3 S_{m12}}{1 + k_6 S_{m11} + k_6 k_7 \det[\mathbf{S}_m] + k_7 S_{m22}} \\ Y_{x21} &= -\frac{k_3 S_{m21}}{1 + k_6 S_{m11} + k_6 k_7 \det[\mathbf{S}_m] + k_7 S_{m22}} \\ Y_{x22} &= \frac{k_4 + k_4 k_6 S_{m11} + k_5 k_6 \det[\mathbf{S}_m] + k_5 S_{m22}}{1 + k_6 S_{m11} + k_6 k_7 \det[\mathbf{S}_m] + k_7 S_{m22}} \end{aligned} \tag{8}$$

The seven coefficients k_1, k_2, k_3, k_4, k_5, k_6, k_7 in (8) are defined as

$$\begin{aligned} k_1 &= \frac{-A_1 + C_1 Z_0}{B_1 - D_1 Z_0},\ k_2 = \frac{A_1 + C_1 Z_0}{B_1 - D_1 Z_0}, \\ k_3 &= -\frac{2Z_0}{\left(B_1 - D_1 Z_0\right)\left(B_2 - D_2 Z_0\right)}, \\ k_4 &= \frac{-A_2 + C_2 Z_0}{B_2 - D_2 Z_0},\ k_5 = \frac{A_2 + C_2 Z_0}{B_2 - D_2 Z_0}, \\ k_6 &= \frac{B_1 + D_1 Z_0}{-B_1 + D_1 Z_0},\ k_7 = \frac{B_2 + D_2 Z_0}{-B_2 + D_2 Z_0} \end{aligned} \tag{9}$$

The eight ABCD parameters representing the two probes are not standard information in data-sheets, and their determination would require ad-hoc characterization setups for each probe. Following the same approach of the SPS [13], [26], it is simpler and time saving to establish an overall calibration procedure aimed at the direct experimental determination of the seven coefficients (9), which are then directly used in (8).

Published version available, doi: 10.1109/TIE.2024.3357888.

B. Calibration Procedure

Preliminarily, it is worth observing that the fully coupled equations (8) degenerate into separate equations if the two ports are uncoupled, that is, if the two-port network is composed of separate one-port admittances. Indeed, in such a case $S_{m12} = S_{m21} = 0$, hence obviously $Y_{x12} = Y_{x21} = 0$ in (8). Additionally, after basic algebra, self-admittances can be expressed as

$$Y_{x11}\big|_{S_{m12}=S_{m21}=0} = \frac{k_1 + k_2 S_{m11}}{1 + k_6 S_{m11}} \tag{10}$$

$$Y_{x22}\big|_{S_{m21}=S_{m12}=0} = \frac{k_4 + k_5 S_{m22}}{1 + k_7 S_{m22}} \tag{11}$$

which noteworthily represent an alternative formulation of the equations of the SPS [13], [26] at each separate port. Hence, one can adapt the same SPS calibration procedure [13], carried out twice. Namely, the calibration procedure is based on the availability of three one-port reference loads, whose admittances Y_A, Y_B, Y_C are known. By connecting in turn these loads to probe 1, the reflection S-parameters S_{1A}, S_{1B}, S_{1C}, respectively, are measured by the VNA at port 1. Then, by enforcing (10), a linear system in the variables k_1, k_2, k_6 is obtained as

$$\begin{cases} Y_A\left(1 + k_6 S_{1A}\right) = k_1 + k_2 S_{1A} \\ Y_B\left(1 + k_6 S_{1B}\right) = k_1 + k_2 S_{1B} \\ Y_C\left(1 + k_6 S_{1C}\right) = k_1 + k_2 S_{1C} \end{cases} \tag{12}$$

which yields one unique solution in the form

$$k_1 = \frac{Y_A\left(Y_B - Y_C\right)S_{1B}S_{1C} + Y_B\left(Y_C - Y_A\right)S_{1C}S_{1A} + Y_C\left(Y_A - Y_B\right)S_{1A}S_{1B}}{S_{1A}S_{1B}\left(Y_A - Y_B\right) + S_{1B}S_{1C}\left(Y_B - Y_C\right) + S_{1C}S_{1A}\left(Y_C - Y_A\right)} \tag{13}$$

$$k_2 = \frac{Y_A\left(Y_B - Y_C\right)S_{1A} + Y_B\left(Y_C - Y_A\right)S_{1B} + Y_C\left(Y_A - Y_B\right)S_{1C}}{S_{1A}S_{1B}\left(Y_A - Y_B\right) + S_{1B}S_{1C}\left(Y_B - Y_C\right) + S_{1C}S_{1A}\left(Y_C - Y_A\right)} \tag{14}$$

$$k_6 = \frac{\left(Y_B - Y_C\right)S_{1A} + \left(Y_C - Y_A\right)S_{1B} + \left(Y_A - Y_B\right)S_{1C}}{S_{1A}S_{1B}\left(Y_A - Y_B\right) + S_{1B}S_{1C}\left(Y_B - Y_C\right) + S_{1C}S_{1A}\left(Y_C - Y_A\right)} \tag{15}$$

Similarly, by connecting in turn the reference admittances Y_A, Y_B, Y_C to probe 2, the corresponding reflection S-parameters S_{2A}, S_{2B}, S_{2C} are measured by the VNA at port 2. Hence, by enforcing (11) a linear system in the variables k_4, k_5, k_7 is obtained as

$$\begin{cases} Y_A\left(1 + k_7 S_{2A}\right) = k_4 + k_5 S_{2A} \\ Y_B\left(1 + k_7 S_{2B}\right) = k_4 + k_5 S_{2B} \\ Y_C\left(1 + k_7 S_{2C}\right) = k_4 + k_5 S_{2C} \end{cases} \tag{16}$$

the unique solution of which is

$$k_4 = \frac{Y_A\left(Y_B - Y_C\right)S_{2B}S_{2C} + Y_B\left(Y_C - Y_A\right)S_{2C}S_{2A} + Y_C\left(Y_A - Y_B\right)S_{2A}S_{2B}}{S_{2A}S_{2B}\left(Y_A - Y_B\right) + S_{2B}S_{2C}\left(Y_B - Y_C\right) + S_{2C}S_{2A}\left(Y_C - Y_A\right)} \tag{17}$$

$$k_5 = \frac{Y_A\left(Y_B - Y_C\right)S_{2A} + Y_B\left(Y_C - Y_A\right)S_{2B} + Y_C\left(Y_A - Y_B\right)S_{2C}}{S_{2A}S_{2B}\left(Y_A - Y_B\right) + S_{2B}S_{2C}\left(Y_B - Y_C\right) + S_{2C}S_{2A}\left(Y_C - Y_A\right)} \tag{18}$$

$$k_7 = \frac{\left(Y_B - Y_C\right)S_{2A} + \left(Y_C - Y_A\right)S_{2B} + \left(Y_A - Y_B\right)S_{2C}}{S_{2A}S_{2B}\left(Y_A - Y_B\right) + S_{2B}S_{2C}\left(Y_B - Y_C\right) + S_{2C}S_{2A}\left(Y_C - Y_A\right)} \tag{19}$$

The last coefficient k_3 can be determined by connecting a reference two-port network to the probes, whose known admittance matrix is

$$\mathbf{Y}_D = \begin{bmatrix} Y_{D11} & Y_{D12} \\ Y_{D21} & Y_{D22} \end{bmatrix} \tag{20}$$

and measuring the full S-parameter matrix

$$\mathbf{S}_D = \begin{bmatrix} S_{D11} & S_{D12} \\ S_{D21} & S_{D22} \end{bmatrix} \tag{21}$$

By enforcing data (20), (21) in the mutual admittances (8), coefficient k_3 is readily obtained as

$$\begin{aligned} k_3 &= \frac{1 + k_6 S_{D11} + k_6 k_7 \det[\mathbf{S}_D] + k_7 S_{D22}}{S_{D21}} Y_{D21} = \\ &= \frac{1 + k_6 S_{D11} + k_6 k_7 \det[\mathbf{S}_D] + k_7 S_{D22}}{S_{D12}} Y_{D12} \end{aligned} \tag{22}$$

Note that the alternative expressions in (22) coincide for reciprocal reference networks since $S_{D12} = S_{D21}$, $Y_{D12} = Y_{D21}$.

III. Experimental Validation

A. Experimental Setup

The first step for the validation of the proposed method is selecting a couple of suitable probes. Commonly available probes developed for completely different purposes (e.g. bulk current injection (BCI) probes designed to inject radio frequency interference, or monitor probes designed for current measurement) can be used in the proposed application, provided that the frequency range of interest for admittance measurement is within the probe nominal specifications. In particular, the experimental setup sketched in Fig. 1 is realized by means of a Keysight E5061B VNA, connected to two inductive probes by coaxial cables. Probe 1 is a BCI probe FCC F-120-2 and probe 2 is a monitor probe Solar 9123-1N, chosen for no other reasons than availability. To match the secondary turns with the unchangeable primary turns inside the probe, so to optimize measurement sensitivity [13], probe 1 and 2 are clamped on two turns and six turns of wire, respectively (in this respect, probes with only one primary turn would be more practical). Once probes are chosen, any parameter and any deviation (e.g., versus frequency) is accounted for by the calibration procedure in Sec. III.B.

The VNA is set to measure 1601 points from 150 kHz to 30 MHz, with 100 Hz resolution bandwidth, and 8 dBm forward power. A VNA short-open-load-thru calibration procedure is preliminarily carried out to account for coaxial cables.

B. Probe Calibration

Each probe is firstly calibrated by one-port measurements (Fig. 2(a)). The final two-port calibration measurement is simply realized by connecting the probes secondary windings as shown in Fig. 2(b), with the longitudinal insertion of a reference load Y_D, determining an admittance matrix (20) where $Y_{D11} = Y_{D22} = Y_D$, $Y_{D12} = Y_{D21} = -Y_D$. Note that the wire turns around each probe are realized with a marked terminal in order to visualize the probes mutual orientation and keep it consistent during the experimental campaign. In principle, any load values could be used for calibration according to Sec. II.B. However, from a practical perspective, the required reference admittances must ensure that the linear systems (12),

Published version available, doi: 10.1109/TIE.2024.3357888.

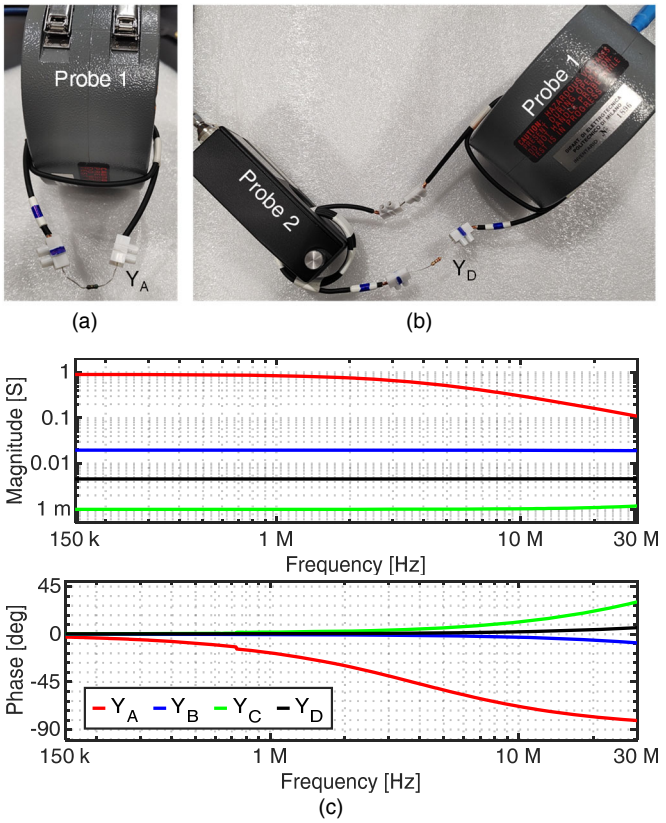

Fig. 2. (a) One-port calibration setup with BCI probe, (b) two-port calibration setup, and (c) admittance magnitude and phase of the reference resistors.

(16) involved in the calibration procedure are determined. This is granted only if: 1) magnitudes are very different and span (with four samples only) the magnitude range of interest for measurement; 2) magnitude difference is maintained and well controlled in the whole frequency range of interest. Resistors easily cope with these requirements as their frequency response is almost constant. Hence, four reference loads are chosen as resistors of nominal values 1.1 Ω, 50 Ω, 1 kΩ, 220 Ω, whose admittances Y_A, Y_B, Y_C, Y_D, respectively (plotted in Fig. 2(c)), are known by independent reflectometric measurements carried out by an impedance analyzer, and include the effect of parasitics (series inductance, parallel capacitance). A flowchart summarizing the sequence of operations comprised in the proposed calibration procedure is reported in Fig. 3. The magnitude and phase of coefficients k_1, k_2, k_3, k_4, k_5, k_6, k_7 obtained from the calibration procedure are plotted in Fig. 4.

C. Verification

In order to verify the proposed measurement method, two passive test networks called symmetrical (SYM) and asymmetrical (ASYM) have been constructed, whose circuit can be seen in Fig. 5, along with a principle representation of the whole setup. Each test network is a three-port network with $R_1 = R_2 = 75$ Ω (SYM) or $R_1 = 0$ Ω, $R_2 = 125$ Ω (ASYM), which is used as two-port network by terminating the third port with a resistor (50 Ω), an inductor (10 μH), or a capacitor (47 nF). Test networks are enclosed in metallic boxes with external SMA connectors, which enable direct VNA connection to measure S-parameters. The latter can be

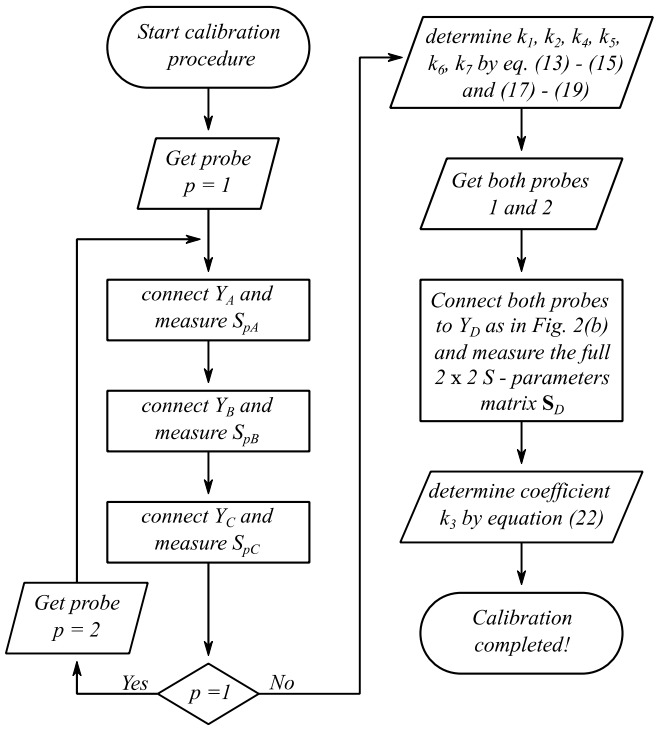

Fig. 3. Flowchart representing the main steps of the proposed calibration procedure.

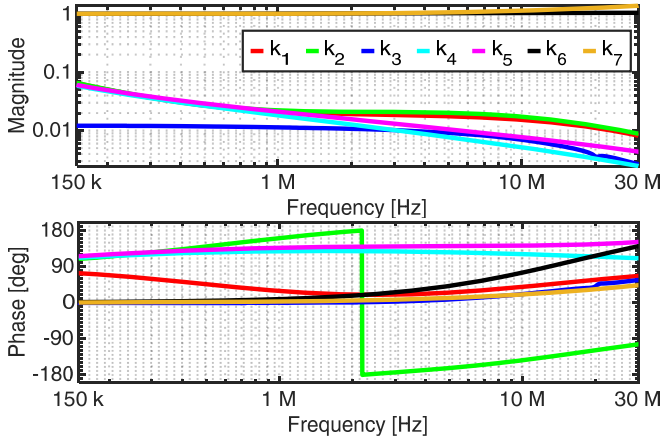

Fig. 4. Magnitude of coefficients k_1, k_2, k_3, k_4, k_5 [S], k_6, k_7 [unitless] obtained from the calibration procedure, and their angle.

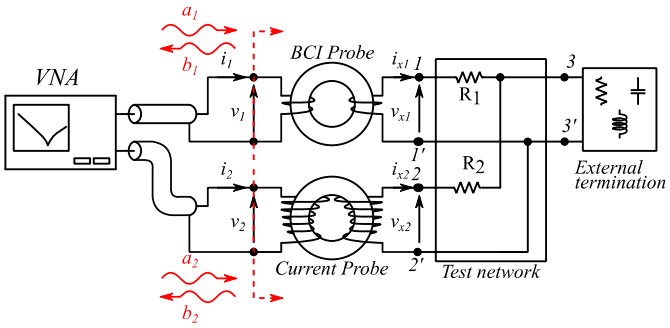

Fig. 5. Principle representation of the experimental setup for calibration and verification.

converted into admittances (2) to be used as reference values for validation. As shown in Fig. 6, the connection of the test networks to the probes needs two short pieces of twisted-wire pair which have been separately characterized, in terms of

Published version available, doi: 10.1109/TIE.2024.3357888.

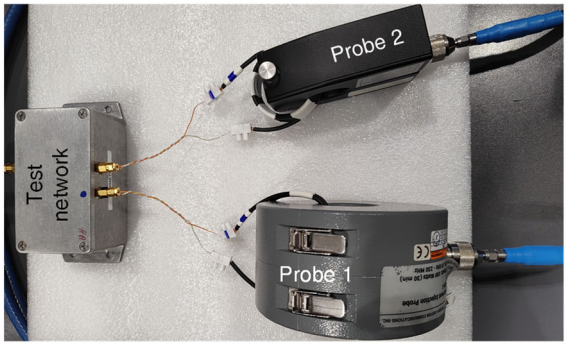

Fig. 6. Experimental setup for verification of the proposed admittance measurement method on passive test loads.

lumped capacitance and inductance, to allow for embedding their contribution to the reference admittance values.

The set of Figures 7-12 shows the comparison between reference values and admittance parameters obtained by the proposed inductively coupled measurement method, in magnitude and phase. Specifically, Fig. 7, Fig. 9 and Fig. 11, refer to SYM with resistive, capacitive and inductive termination, respectively. Fig. 8, Fig. 10 and Fig. 12 refer to ASYM with resistive, capacitive and inductive termination, respectively. Lastly, Table I reports the main error estimators, namely maximum and average error, and standard deviation, for the measurements corresponding to Figures 7 - 12.

The overall accuracy of the proposed measurement method is very good over the frequency range of interest. The dynamic range extends over six orders of magnitude from tens of micro-siemens to some siemens. The variable frequency response of phases is well captured in the six validation cases.

IV. In-Circuit Admittance Parameters of a Single-Phase Motor Drive System

In this Section, an application example of the use of the proposed inductively coupled measurement method for EMI analysis is discussed. In particular, the admittance matrix $\mathbf{Y}_{MDS}$ of a single-phase MDS is involved in the equivalent representation of the passive part of a Norton circuit model,

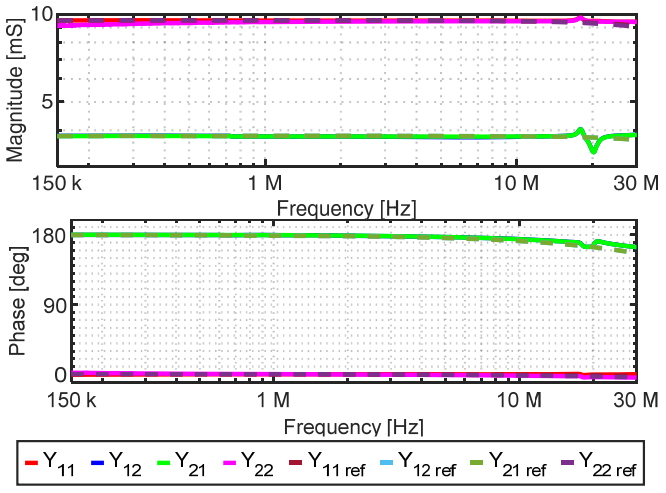

Fig. 7. Comparison between reference (dashed lines) and measured (solid lines) values of the coefficients of the admittance matrix of the SYM test load with resistive termination.

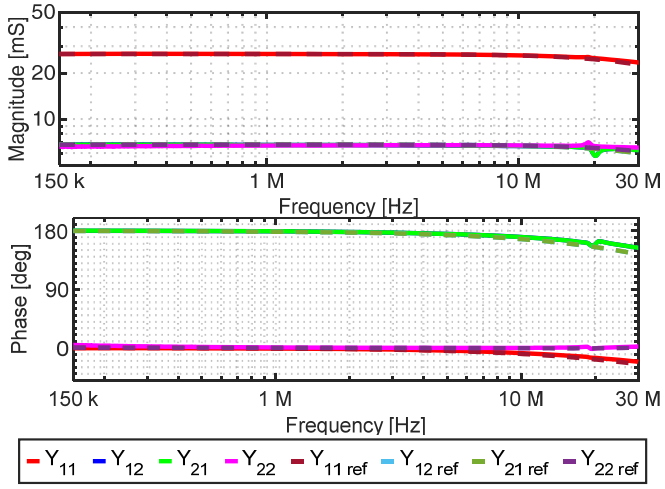

Fig. 8. Comparison between reference (dashed lines) and measured (solid lines) values of the coefficients of the admittance matrix of the ASYM test load with resistive termination.

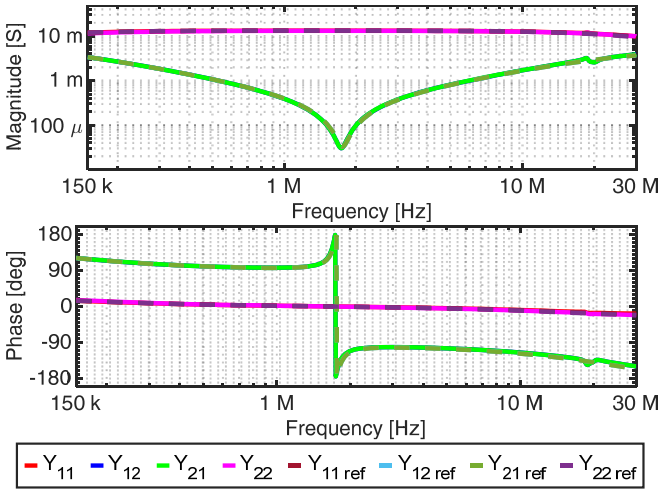

Fig. 9. Comparison between reference (dashed lines) and measured (solid lines) values of the coefficients of the admittance matrix of the SYM test load with capacitive termination.

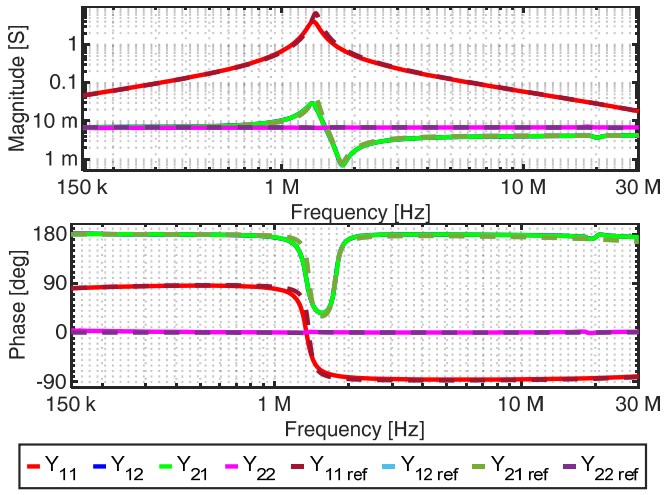

Fig. 10. Comparison between reference (dashed lines) and measured (solid lines) values of the coefficients of the admittance matrix of the ASYM test load with capacitive termination.

Published version available, doi: 10.1109/TIE.2024.3357888.

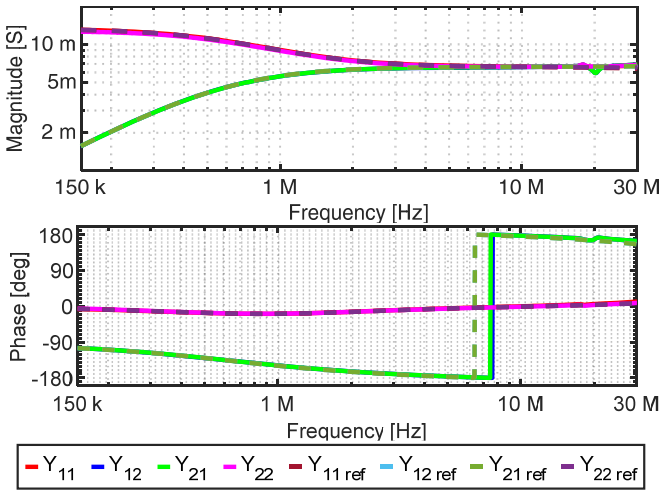

Fig. 11. Comparison between reference (dashed lines) and measured (solid lines) values of the coefficients of the admittance matrix of the SYM test load with inductive termination.

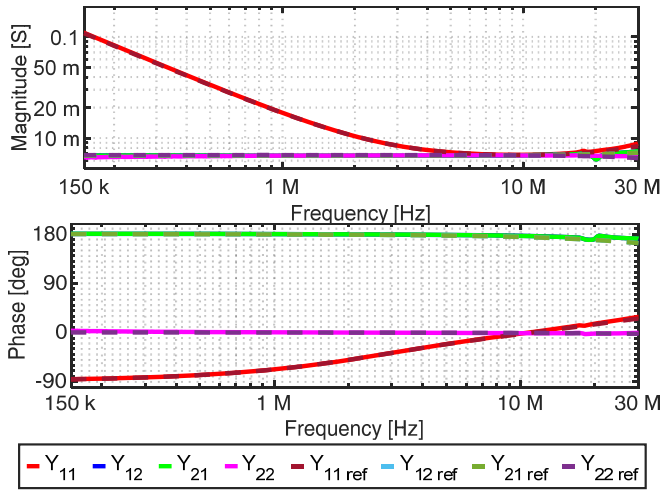

Fig. 12. Comparison between reference (dashed lines) and measured (solid lines) values of the coefficients of the admittance matrix of the ASYM test load with inductive termination.

TABLE I
OVERVIEW OF MAXIMUM AND AVERAGE MEASUREMENT ERRORS

Case	Parameter	Max Magnitude Error [%]	Max Angle Error [°]	Average Magnitude Error [%]	Average Angle Error [°]	Magnitude Standard Deviation [%]	Phase Standard Deviation [°]
Symmetrical Resistive	Y_{11}	3.834	1.876	0.262	0.222	0.564	0.393
	Y_{22}	4.319	2.008	-0.851	0.114	3.467	0.381
	Y_m	10.83	8.350	-0.219	1.509	2.281	5.992
Asymmetrical Resistive	Y_{11}	3.786	3.753	0.376	0.581	0.696	1.448
	Y_{22}	8.271	4.165	-0.501	0.938	3.931	1.785
	Y_m	9.960	10.05	-0.244	2.006	2.043	10.23
Symmetrical Capacitive	Y_{11}	5.180	1.838	0.061	0.206	0.299	0.185
	Y_{22}	6.903	1.953	-0.777	0.273	3.417	0.302
	Y_m	15.91	15.07	0.898	1.787	15.94	9.377
Asymmetrical Capacitive	Y_{11}	47.01	37.18	-1.464	-0.059	50.98	21.13
	Y_{22}	7.104	3.822	-0.708	0.797	3.926	1.409
	Y_m	46.50	36.44	-2.382	1.293	58.23	27.62
Symmetrical Inductive	Y_{11}	6.728	3.766	0.594	0.479	1.674	1.085
	Y_{22}	11.03	8.381	-0.696	0.190	3.184	0.197
	Y_m	5.657	1.409	-0.268	1.487	1.925	5.896
Symmetrical Inductive	Y_{11}	6.154	2.915	0.827	0.435	1.783	0.574
	Y_{22}	5.447	3.073	-1.095	0.447	4.734	0.913
	Y_m	10.96	8.234	-0.217	1.447	1.981	5.486

which, unitedly with suitable current sources I_{NP} and I_{NN}, describes the converter as a multiport EMI source in the frequency domain [14], [15], as shown in Fig. 13. In this respect, the proposed inductively coupled in-circuit measurement method offers a straightforward solution to obtain the passive part of such a behavioral model.

A. Experimental Setup

The experimental setup is shown in Fig. 14(a). Namely, the EUT is an MDS which is comprised of a cabinet containing a single-phase electronic converter (driving a three-phase asynchronous motor, not shown), fed by a Line Impedance Stabilization Network (LISN) through a cable with phase (P), neutral (N) and protective earth (PE) wires. The LISN is fed by the building 50 Hz power outlet. The VNA is set to measure 1601 points from 150 kHz to 30 MHz, with 100 Hz resolution bandwidth, and 8 dBm forward power. The high power level is selected in order to provide a measurement signal much stronger than the EUT conducted emission sources (I_{NP} and I_{NN} in Fig. 13) in the frequency range of interest. Probes 1 and 2 are clamped just out of the cabinet on two and six turns of wires P and N, respectively, as shown in Fig. 14(b). This setup enables in-circuit measurement of admittance parameters during the standard operation of the MDS. In particular, the MDS is characterized with: a) power line off, which is the only measurement which could be performed with other measurement methods; b) power line on, stand-by operation (converter on, but motor not driven); c) power line on and converter driving the motor. In this last condition, a number of different converter switching frequencies has been tested in order to assess the impact of this parameter on the converter admittance parameters.

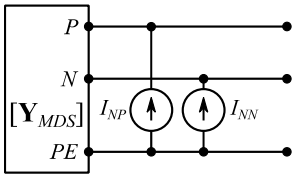

Fig. 13. Behavioral model of an electronic power converter in form of two-port Norton circuit model.

Published version available, doi: 10.1109/TIE.2024.3357888.

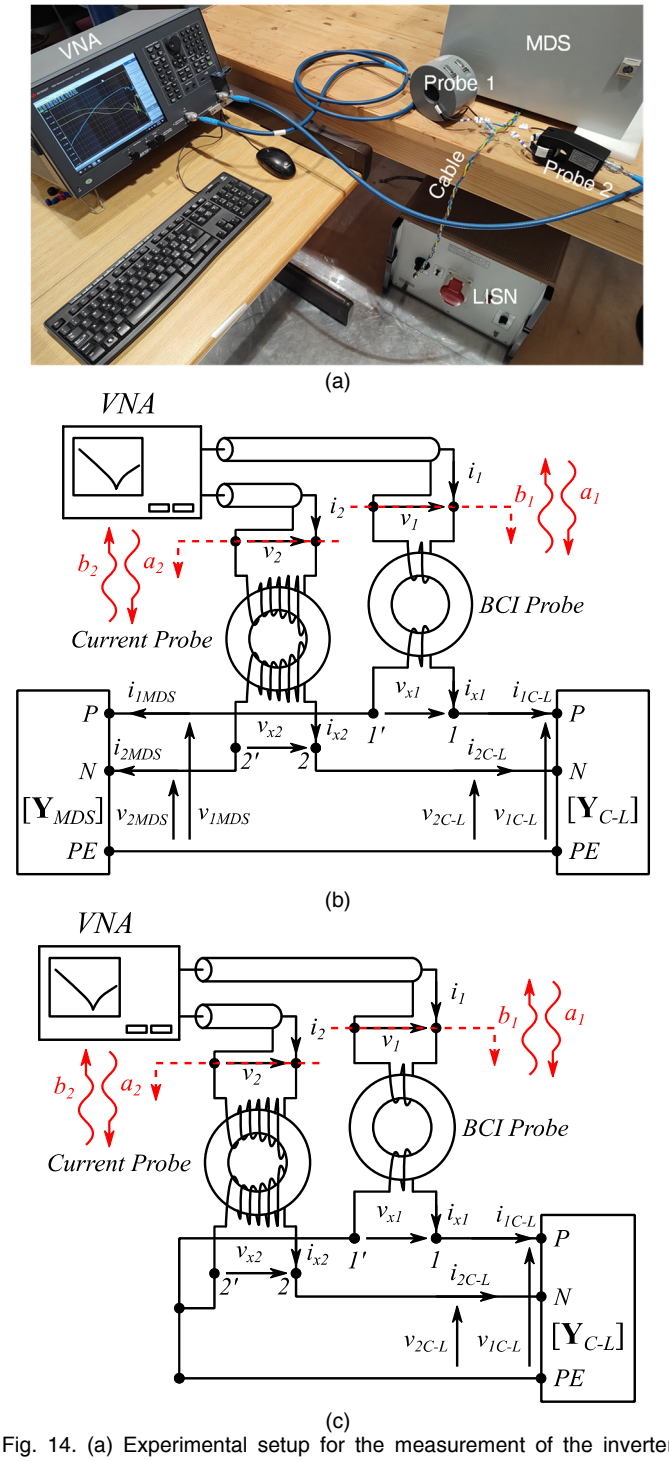

Fig. 14. (a) Experimental setup for the measurement of the inverter output admittance matrix, (b) its principle schematic, and (c) reduced setup for LISN and cable characterization.

A reduced setup shown in Fig. 14(c) is used to separately measure the powerline (i.e., cable and LISN) admittance parameters. In this setup, the MDS is disconnected, and its P and N wires are shorted to PE (while the LISN is clearly not fed by the power outlet).

B. In-Circuit Admittance Measurement and de-embedding

The proposed measurement method is performed in the two setups shown in Fig. 14(b) and Fig. 14(c). As a result, two admittance matrices in the frequency range 150 kHz – 30 MHz were evaluated. It is worth recalling that these are admittances seen at the two longitudinal ports created by clamping the probes along P and N wires. For the test setup reported in Fig. 14(b), the whole circuital loop (MDS, cable, LISN) contributes to such admittances, hence, the measured admittance matrix is hereby denoted as $\mathbf{Y}_{loop}$. For the second test setup, reported in Fig. 14(c), the admittance matrix receives contributions from the cable and LISN only, and is hereby called $\mathbf{Y}_{C\text{-}L}$.

To retrieve the MDS admittance matrix $\mathbf{Y}_{MDS}$, the cable and LISN contributions must be de-embedded from the whole loop. With reference to variables depicted in Fig. 14(b), the following relationships hold:

$$\mathbf{i}_{MDS} = \mathbf{Y}_{MDS}\mathbf{v}_{MDS} \tag{23}$$

$$\mathbf{i}_{C-L} = \mathbf{Y}_{C-L}\mathbf{v}_{C-L} \tag{24}$$

$$\mathbf{i}_{x} = \mathbf{Y}_{loop}\mathbf{v}_{x} \tag{25}$$

where $\mathbf{i}_{MDS} = [i_{1MDS}\ i_{2MDS}]^{\mathrm{T}}$, $\mathbf{v}_{MDS} = [v_{1MDS}\ v_{2MDS}]^{\mathrm{T}}$, $\mathbf{i}_{C\text{-}L} = [i_{1C\text{-}L}\ i_{2C\text{-}L}]^{\mathrm{T}}$, $\mathbf{v}_{C\text{-}L} = [v_{1C\text{-}L}\ v_{2C\text{-}L}]^{\mathrm{T}}$, $\mathbf{i} = [i_{x1}\ i_{x2}]^{\mathrm{T}}$, $\mathbf{v} = [v_{x1}\ v_{x2}]^{\mathrm{T}}$. Considering the circuit in Fig. 14(b), it is possible to appreciate that the following Kirchhoff laws hold:

$$\mathbf{i}_{x} = \mathbf{i}_{C-L} = -\mathbf{i}_{MDS} \tag{26}$$

$$\mathbf{v}_{x} = \mathbf{v}_{C-L} - \mathbf{v}_{MDS} \tag{27}$$

Combining (23)-(27) , it is easy to prove that the MDS admittance matrix is obtained as

$$\mathbf{Y}_{MDS} = \left(\mathbf{Y}_{loop}^{-1} - \mathbf{Y}_{C-L}^{-1}\right)^{-1} \tag{28}$$

C. Motor Drive System Admittance Parameters

By means of the method proposed in Section II and of the LISN and cables de-embedding procedure discussed in Section IV.B, the admittance matrix $\mathbf{Y}_{MDS}$ of the single-phase converter depicted in Fig. 14(a) is obtained. The magnitude and phase of the elements of $\mathbf{Y}_{MDS}$ are reported in Fig. 15. Specifically, the self-admittance measured from port 1 is reported in Fig. 15(a), the mutual admittance is reported in Fig. 15(b) (only one mutual parameter $Y_M = Y_{12} = Y_{21}$ is shown as the resulting admittance matrix turns out to be reciprocal), and the self-admittance measured from port 2 is reported in Fig. 15(c).

The MDS admittance matrix has been measured in different operating conditions, namely: powerline turned off, stand-by (i.e., MDS turned on and motor stopped), and motor driven with different switching frequencies (2 kHz, 5 kHz, 10 kHz and 15 kHz) of the inverter inside the MDS. One can note that, in all operating conditions, the self-admittances are very similar, which is consistent with the symmetrical construction usually found in single-phase converters and relative EMI input filters. Additionally, the admittance parameters are scarcely dependent on switching frequency, slightly change between stand-by and motor-driven conditions and are very different from the admittances measured with no power. This is one of the main reasons of interest towards in-circuit measures, as the latter could be directly measured by any other methods, but would also be the least representative of the EUT in real operating condition.

Published version available, doi: 10.1109/TIE.2024.3357888.

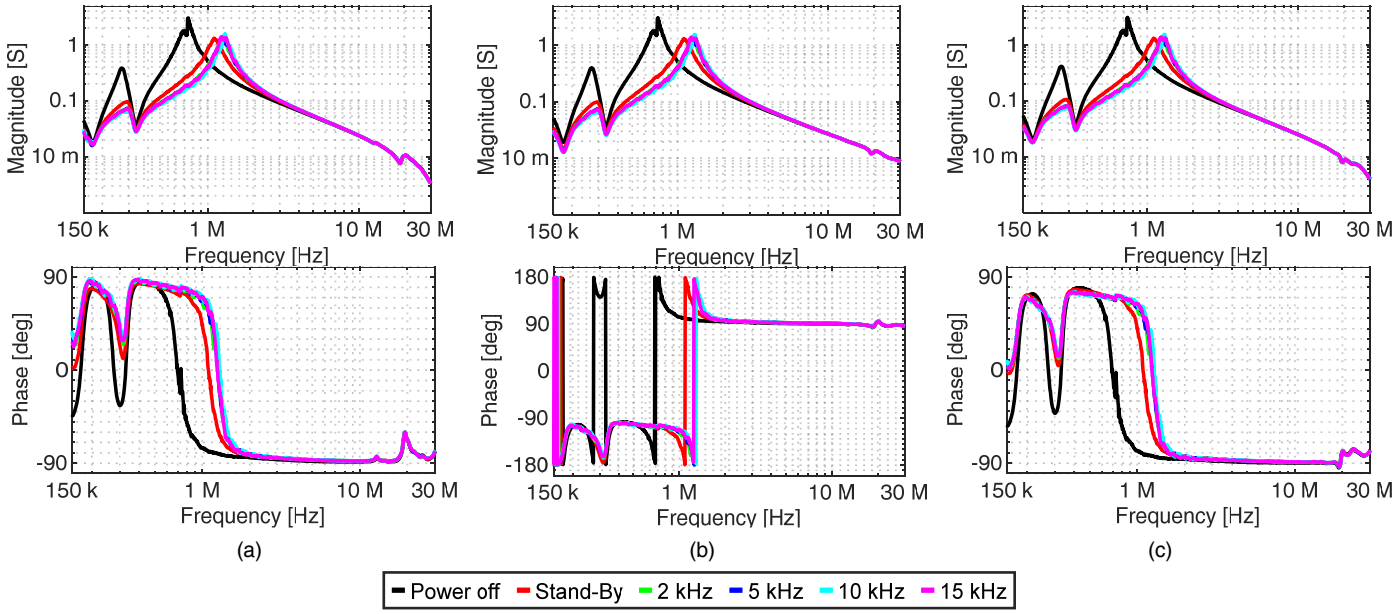

Fig. 15. Comparison between admittance matrix elements Y_{11} (a), Y_M (c), Y_{22} (c) in different operating conditions: power line off (black), stand-by (red), and switching frequency equal to 2 kHz (green), 5 kHz (blue), 10 kHz (cyan), 15 kHz (magenta).

D. Motor Drive System Behavioral Circuit Model

As mentioned, the admittance matrix of a power converter is involved in the equivalent representation of the passive part of a Norton circuit model in the frequency domain [14], [15], and can be directly obtained by means of the proposed inductively coupled in-circuit measurement method.

Indeed, the voltage-controlled form (23), for a reciprocal two port-network, inherently describe the circuit model in Fig. 16, which consists of three admittances

$$Y_{eq1} = Y_{MDS\,11} + Y_{MDS\,M} \tag{29}$$

$$Y_{eq2} = Y_{MDS\,22} + Y_{MDS\,M} \tag{30}$$

$$Y_{eqM} = -Y_{MDS\,M} \tag{31}$$

It is worth nothing that this admittance-based modeling procedure can be extended to an EUT with an arbitrary number N of ports: first, the proposed measurement procedure is repeated two ports at a time, until all the elements of the $N\times N$ admittance matrix are found (indeed, when no probe is clamped on a wire, that port along the wire is in short-circuit condition). Second, a behavioral circuit model composed of lumped admittances is constructed with the same rationale as (29)-(31).

V. Conclusion

In this paper, a novel inductively coupled two-port in-circuit admittance measurement method is proposed. The proposed method provides accurate measurement of 2×2 admittance matrix, including mutual terms, whereas previous methods are limited to the measurement of a single impedance. Additionally, it can be used both on passive or energized EUT. The proposed method requires a VNA and two clamp-on inductive probes of any kind (e.g., BCI or monitor). The S-parameters measured by the VNA are transformed into the admittance parameters of the EUT by algebraic equations involving seven coefficients, which are preliminary determined by a simple calibration procedure exploiting four reference resistors. This method has been experimentally validated for a set of artificial passive networks, then applied to the measurement of the admittance matrix of a real single-phase MDS, in the frequency range 150 kHz – 30 MHz. Additionally, a straightforward procedure to de-embed the powerline contribution to the measured MDS admittance has been presented. Unlike impedance parameters, the measured admittance matrix naturally describes an equivalent behavioral circuit model in frequency domain, which can be extended to an arbitrary number of ports.

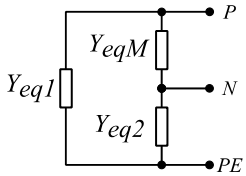

Fig. 16. Topology of the admittance matrix behavioral model.

References

[1] X. Zhang, X. Ruan, and Q.-C. Zhong, “Improving the stability of cascaded DC/DC converter systems via shaping the input impedance of the load converter with a parallel or series virtual impedance,” *IEEE Trans. Ind. Electron.*, vol. 62, no. 12, pp. 7499–7512, Dec. 2015.

[2] P. Pan, H. Hu, X. Yang, F. Blaabjerg, X. Wang, and Z. He, “Impedance measurement of traction network and electric train for stability analysis in high-speed railways,” *IEEE Trans. Power Electron.*, vol. 33, no. 12, pp. 10086–10100, Dec. 2018.

[3] B. Hu, H. Nian, M. Li, Y. Liao, J. Yang and H. Tong, "Impedance Characteristic Analysis and Stability Improvement Method for DFIG System Within PLL Bandwidth Based on Different Reference Frames," in *IEEE Trans. on Ind. Electron.*, vol. 70, no. 1, pp. 532-543, Jan. 2023.

[4] S. B. Lee, R. M. Tallam, and T. G. Habetler, “A robust, on-line turnfault detection technique for induction machines based on monitoring the sequence component impedance matrix,” *IEEE Trans. Power Electron.*, vol. 18, no. 3, pp. 865–872, May 2003.

Published version available, doi: 10.1109/TIE.2024.3357888.

[5] Z. Zhao, F. Fan, W. Wang, Y. Liu, and K. Y. See, “Detection of stator interturn short-circuit faults in inverter-fed induction motors by online common-mode impedance monitoring,” *IEEE Trans. Instrum. Meas.*, vol. 70, 2021, Art. no. 3513110.

[6] J. Sihvo, T. Roinila, and D.-I. Stroe, “Novel fitting algorithm for parametrization of equivalent circuit model of Li-ion battery from broadband impedance measurements,” *IEEE Trans. Ind. Electron.*, vol. 68, no. 6, pp. 4916–4926, Jun. 2021.

[7] E. Mazzola, A. Amaducci, E. F. Bononi, and V. Montanaro, “Measurement of LiFePO4 battery modal impedances under different conditions,” in *Proc. IEEE Asia-Pacific Symp. Electromagn. Compat.*, 2021, pp. 1–4.

[8] Y. Guo, Y. Zhang, W. Zhang, and L. Wang, “Battery parameter identification based on wireless power transfer system with rectifier load,” *IEEE Trans. Ind. Electron.*, vol. 68, no. 8, pp. 6893–6904, Aug. 2021.

[9] F. Fan, K. Y. See, X. Liu, K. Li and A. K. Gupta, "Systematic Common-Mode Filter Design for Inverter-Driven Motor System Based on In-Circuit Impedance Extraction," in *IEEE IEEE Trans. Electromagn. Compat.*, vol. 62, no. 5, pp. 1711-1722, Oct. 2020.

[10] V. Tarateeraseth, K. Y. See, F. G. Canavero, and R.W.-Y. Chang, “Systematic electromagnetic interference filter design based on information from in-circuit impedance measurements,” *IEEE Trans. Electromagn. Compat.*, vol. 52, no. 3, pp. 588–598, Aug. 2010.

[11] S. Negri, G. Spadacini, F. Grassi and S. A. Pignari, "Black-Box Modeling of EMI Filters for Frequency and Time-Domain Simulations," in *IEEE Trans. Electromagn. Compat.*, vol. 64, no. 1, pp. 119-128, Feb. 2022.

[12] S. Negri, G. Spadacini, F. Grassi and S. A. Pignari, "Prediction of EMI Filter Attenuation in Power-Electronic Converters via Circuit Simulation," in *IEEE Trans. Electromagn. Compat.*, vol. 64, no. 4, pp. 1086-1096, Aug. 2022.

[13] L. Wan, S. Negri, G. Spadacini, F. Grassi, and S. A. Pignari, “Enhanced Impedance Measurement to Predict Electromagnetic Interference Attenuation Provided by EMI Filters in Systems with AC/DC Converters,” *Applied Sciences*, vol. 12, no. 23, p. 12497, Dec. 2022.

[14] A. C. Baisden, D. Boroyevich, and W. Fei, “Generalized terminal modeling of electromagnetic interference,” *IEEE Trans. Ind. Appl.*, vol. 46, no. 5, pp. 2068–2079, Sep./Oct. 2010.

[15] H. Bishnoi, A. C. Baisden, P. Mattavelli and D. Boroyevich, "Analysis of EMI Terminal Modeling of Switched Power Converters," in *IEEE Trans. on Power Electron.,* vol. 27, no. 9, pp. 3924-3933, Sept. 2012.

[16] Z. Zhao, A. Weerasinghe, W. Wang, E. K. Chua, and K. Y. See, “Eliminating the effect of probe-to-probe coupling in inductive coupling method for in-circuit impedance measurement,” *IEEE Trans. Instrum. Meas.*, vol. 70, 2021, Art. no. 1000908.

[17] S. Cobreces, E. J. Bueno, D. Pizarro, F. J. Rodriguez, and F. Huerta, “Grid impedance monitoring system for distributed power generation electronic interfaces,” *IEEE Trans. Instrum. Meas.*, vol. 58, no. 9, pp. 3112–3121, Sep. 2009.

[18] H. Hu, P. Pan, Y. Song, and Z. He, “A novel controlled frequency band impedance measurement approach for single-phase railway traction power system,” *IEEE Trans. Ind. Electron.*, vol. 67, no. 1, pp. 244–253, Jan. 2020.

[19] M. Li, H. Nian, B. Hu, Y. Xu, Y. Liao, and J. Yang, “Design method of multi-sine signal for broadband impedance measurement considering frequency coupling characteristic,” *IEEE J. Emerg. Sel. Topics Power Electron.*, vol. 10, no. 1, pp. 532–543, Feb. 2022.

[20] T. Funaki, N. Phankong, T. Kimoto, and T. Hikihara, “Measuring terminal capacitance and its voltage dependency for high-voltage power devices,” *IEEE Trans. Power Electron.*, vol. 24, no. 6, pp. 1486–1493, Jun. 2009.

[21] X. Shang, D. Su, H. Xu, and Z. Peng, “A noise source impedance extraction method for operating SMPS using modified LISN and simplified calibration procedure,” *IEEE Trans. Power Electron.*, vol. 32, no. 6, pp. 4132–4139, Jun. 2017.

[22] Z. Zhao et al., “Voltage-dependent capacitance extraction of SiC power MOSFETs using inductively coupled in-circuit impedance measurement technique,” *IEEE Trans. Electromagn. Compat.*, vol. 61, no. 4, pp. 1322–1328, Aug. 2019.

[23] K. R. Li, K. Y. See, and X. M. Li, “Inductive coupled in-circuit impedance monitoring of electrical system using two-port ABCD network approach,” *IEEE Trans. Instrum. Meas.,* vol. 64, no. 9, pp. 2489–2495, Sep. 2015.

[24] S. B. Rathnayaka *et al.*, “Inductively coupled on-line impedance measurement for condition monitoring of electrical equipment,” *IET Sci., Meas. Tech.,* vol. 12, no. 3, pp. 382–387, May 2018.

[25] V.Tarateeraseth, B. Hu, K.Y. See, and F. G. Canavero, “Accurate extraction of noise source impedance of an SMPS under operating conditions,” *IEEE Trans. Power Electron.,* vol. 25, no. 1, pp. 111–117, Jan. 2010.

[26] A. Weerasinghe, Z. Zhao, N. B. Narampanawe, Z. Yang, T. Svimonishvili, and K. Y. See, “Single-probe inductively coupled in-circuit impedance measurement,” *IEEE Trans. Electromagn. Compat.*, vol. 64, no. 1, pp. 2–10, Feb. 2022.

[27] A. Weerasinghe *et al*., "A Novel Single-Probe Setup for Multifrequency Simultaneous Measurement of In-Circuit Impedance," in *IEEE Trans. Ind. Electron.*, vol. 70, no. 9, pp. 9538-9549, Sept. 2023.

[28] R. A. Southwick and W. C. Dolle, “Line impedance measuring instrumentation utilizing current probe coupling,” *IEEE Trans. Electromagn. Compat.*, vol. 13, no. 4, pp. 31–36, Nov. 1971.

[29] S. B. Rathnayaka, K. Y. See, and K. Li, “Online impedance monitoring of transformer based on inductive coupling approach,” *IEEE Trans. Dielectrics Elect. Insul.*, vol. 24, no. 2, pp. 1273–1279, Apr. 2017.

[30] M. Prajapati, F. Fan, Z. Zhao, and K. Y. See, “Estimation of radiated emissions from PV system through black box approach,” *IEEE Trans. Instrum. Meas.*, vol. 70, 2021, Art. no. 9004304.

[31] Z. Zhao *et al*., "In-Circuit Impedance Measurement Setups of Inductive Coupling Approach: A Review," *2022 Asia-Pacific International Symposium on Electromagnetic Compatibility (APEMC)*, Beijing, China, 2022, pp. 228-230.

[32] A. Weerasinghe, Z. Zhao, F. Fan, P. Tu and K. Y. See, "In-Circuit Differential-Mode Impedance Extraction at the AC Input of a Motor Drive System," *2021 Asia-Pacific International Symposium on Electromagnetic Compatibility (APEMC)*, Nusa Dua - Bali, Indonesia, 2021, pp. 1-4.

[33] Z. Zhao, F. Fan, A. Weerasinghe, P. Tu and K. Y. See, "Measurement of In-Circuit Common-Mode Impedance at the AC Input of a Motor Drive System," *2021 Asia-Pacific International Symposium on Electromagnetic Compatibility (APEMC)*, Nusa Dua - Bali, Indonesia, 2021, pp. 1-4.

[34] S. Negri, G. Spadacini, F. Grassi and S. Pignari, "Measurement-Based Equivalent Circuit Model for Time-Domain Simulation of EMI Filters," *2022 International Symposium on Electromagnetic Compatibility – EMC Europe*, Gothenburg, Sweden, 2022, pp. 793-798.

Simone Negri (M’20) received the B.Sc. and M.Sc. (cum Laude) and PhD (cum Laude) degrees in Electrical Engineering from Politecnico di Milano, Milan, Italy, in 2014, 2016, and 2020, respectively.

He is currently an Assistant Professor with Department of the Electronics, Information and Bioengineering (DEIB), Politecnico di Milano, where he has been a Postdoctoral Research Fellow from 2019 to 2022. His research interests are mostly in the field of Electromagnetic Compatibility (EMC), and include EMI filters and electronic power converters modelling and conducted emissions evaluation and prediction. Further research interests include power converters modelling and control, application of advanced control and optimization techniques in power systems, hybrid AC/DC distribution systems, and power quality and reliability.

Dr. Negri is the recipient of the 2023 International Union of Radio Science (URSI) “Roberto Sorrentino” Young Scientist Best Paper Award, and he is active in the standardization of LVDC systems as a Member of the CEI (Italian Electrotechnical Committee) CT 320 technical committee, where he is the convenor of the working group GdL1, Member of several IEC SyC LVDC working groups, and Member of the European Commission SET Plan TWG - LVDC.

Published version available, doi: 10.1109/TIE.2024.3357888.

Giordano Spadacini (M'07–SM'16) received the Laurea (M.Sc.) and Ph.D. degrees in electrical engineering in 2001 and 2005, respectively, from Politecnico di Milano, Italy, where he is currently an Associate Professor with the Dept. of Electronics, Information and Bioengineering. His research interests include statistical models for the characterization of interference effects, distributed parameter circuit modeling, experimental procedures and setups for EMC testing, and EMC in aerospace, automotive and railway systems.

Dr. Spadacini is a recipient of the 2005 EMC Transactions Prize Paper Award, the 2016 and the 2021 R. B. Schulz Best EMC Transactions Paper Award, two Best Symposium Paper Awards from the 2015 Asia-Pacific Int. Symp. on EMC (APEMC) and the 2018 Joint IEEE EMC & APEMC Symposium.

Flavia Grassi (M'07–SM'13) received the Laurea (M.Sc.) and Ph.D. degrees in electrical engineering from Politecnico di Milano, Milan, Italy, in 2002 and 2006, respectively.

She is currently a Full Professor in the Department of Electronics, Information and Bioengineering, Politecnico di Milano. From 2008 to 2009, she was with the European Space Agency (ESA), ESA/ESTEC, The Netherlands, as a Research Fellow. Her research interests include distributed-parameter circuit modeling, statistical techniques, characterization of measurement setups for EMC testing (aerospace and automotive sectors), and application of the powerline communications technology in ac and dc lines.

Dr. Grassi received the International Union of Radio Science (URSI) Young Scientist Award in 2008, and the IEEE Young Scientist Award at the 2016 Asia- Pacific International Symposium on EMC (APEMC), the IEEE EMC Society Transactions Prize Paper Award in 2016 and 2021, and the Best Symposium Paper Award at the 2015 and 2018 APEMC. She is currently serving as an Associate Editor of the IEEE Transactions on Electromagnetic Compatibility, IEEE EMC Magazine, IEEE Letters on Electromagnetic Compatibility Practice and Applications, and IEEE Access.

Sergio A. Pignari (M'01–SM'07–F'12) received the Laurea (M.S.) and Ph.D. degrees in electronic engineering from Politecnico di Torino, Turin, Italy, in 1988 and 1993, respectively.

From 1991 to 1998, he was an Assistant Professor with the Dept. of Electronics, Politecnico di Torino, Turin, Italy. In 1998, he joined Politecnico di Milano, Milan, Italy, where he is currently a Full Professor of Circuit Theory and Electromagnetic Compatibility (EMC) at the Dept. of Electronics, Information, and Bioengineering, and Chair of the B.Sc. and M.Sc. Study Programmes in Electrical Engineering, term 2015-20. He is the author or coauthor of more than 200 papers published in international journals and conference proceedings. His research interests are in the field of EMC and include field-to-wire coupling and crosstalk, conducted immunity and emissions in multi-wire structures, statistical techniques for EMC prediction, and experimental procedures and setups for EMC testing. His research activity is mainly related to Aerospace, Automotive, Energy, and Railway industry sectors.

Dr. Pignari is co-recipient of the 2005, 2016, and 2021 IEEE EMC Society Transactions Prize Paper Award, and a 2011 IEEE EMC Society Technical Achievement Award. He is currently serving as an Associate Editor of the IEEE Transactions on Electromagnetic Compatibility. From 2010 to 2015 he served as the IEEE EMC Society Chapter Coordinator. From 2007 to 2009 he was the Chair of the IEEE Italy Section EMC Society Chapter. He served as the Italian URSI Officer for Commission E (Electromagnetic Noise and Interference), term 2015-18. He has been Technical Program Chair of the ESA Workshop on Aerospace EMC since 2009, and a Member of the Technical Program Committee of the Asia Pacific EMC Week since 2010.

Published version available, doi: 10.1109/TIE.2024.3357888.